T-type Calcium Channel Inhibitors Induce Apoptosis in Medulloblastoma Cells Associated With Altered Metabolic Activity

Mohammed Sedeeq
University of Tasmania
Ahmed Maklad
University of Tasmania
Zikai Feng
University of Tasmania
Richard Wilson
University of Tasmania
Nuri Gueven
University of Tasmania
Iman Azimi (iman.azimi@utas.edu.au)
University of Tasmania Sandy Bay Campus https://orcid.org/0000-0001-9477-9999

Research Article

Keywords: Medulloblastoma, T-type calcium channels, mibefradil, NNC-55-0396, metabolic activity, apoptosis

Posted Date: August 9th, 2021

DOI: https://doi.org/10.21203/rs.3.rs-767880/v1

Version of Record: A version of this preprint was published at Molecular Neurobiology on March 4th, 2022. See the published version at https://doi.org/10.1007/s12035-022-02771-0.

Abstract

Medulloblastoma (MB) is the most common malignant paediatric brain tumour. In our previous studies, we developed a novel 3D assay for MB cells and screened of plasma membrane calcium channel modulators. These studies identified T-type (CaV3) channel inhibitors, mibefradil and NNC-55-0396 (NNC) as selective inhibitors of MB cell growth. Mibefradil was originally approved for treatment of hypertension and angina pectoris, and recently successfully completed a Phase I trial for recurrent high-grade glioma. NNC is an analogue of mibefradil with multiple advantages compared to mibefradil that makes it attractive for potential future clinical trials. In this study, we aimed to characterise the effect of mibefradil and NNC on MB cells and elucidate their mechanism of action. This study demonstrates that the induction of toxicity in MB cells is selective to T-type but not to L-type Ca^{2+} channel inhibitors. Addition of CaV3 inhibitors to vincristine sensitised MB cells to this MB chemotherapeutic agent, suggesting a synergistic effect. Furthermore, CaV3 inhibitors induced cell death in MB cells via apoptosis. Supported by proteomics data and cellular assays, apoptotic cell death was associated with reduced mitochondrial membrane potential and reduced ATP levels, which suggests that both compounds alter the metabolism of MB cells. This study offers new insights into the action of mibefradil and NNC and will pave the way to test these molecules or their analogues in pre-clinical MB models alone and in combination with vincristine to assess their suitability as a potential MB therapy.

Introduction

Medulloblastoma (MB) is a primary malignant tumour of the cerebellum that is rarely seen in adults and predominantly occurs in children. Indeed, MB is the most common childhood malignant brain tumour, representing 20% of all paediatric brain cancers (1). Current treatment options include a combined-modality approach of surgical resection, radio- and chemo-therapy. Although these approaches improve survival of MB patients, they are not completely effective, in particular for high-risk MB. In addition, these treatment modalities are associated with adverse events and severe treatment-related morbidities (2). Hence, new treatment options are urgently needed.

MB is categorised into four molecular subgroups of wingless (WNT), sonic hedgehog (SHH), Group 3 and Group 4. Groups 3 and 4 tumours are associated with higher levels of metastasis and worse clinical outcomes than the other two groups (1). Recently, we developed a novel 3D 384-well agar colony formation assay for MB cells of molecular subgroup 3. Using this assay, we screened a panel of plasma membrane calcium channel modulators and identified modulators of the T-type voltage-gated channels, mibefradil and NNC-55-0396, as selective growth inhibitors of MB cells (3). Intriguingly, previous studies demonstrated that mibefradil suppressed the growth and stemness of glioblastoma stem-like cells and enhanced their sensitivity to temozolomide chemotherapy (4). Mibefradil is a selective inhibitor of CaV3 T-type Ca^{2+} channel and was originally approved for treatment of hypertension and angina pectoris. Mibefradil was withdrawn from the market in 1998 due to potential interactions with other drugs frequently taken by patients with cardiovascular diseases. Mibefradil recently successfully completed a Phase I trial for recurrent high-grade glioma. Together with temozolomide, it was well-tolerated in patients

with no signs of toxicity (ClinicalTrials.gov identifier NCT01480050 and publication (5)). NNC55-0396 (NNC) is an analogue of mibefradil with higher blood-brain-barrier permeability (6, 7). In comparison to mibefradil, NNC also shows lower non-specific effects on L-type calcium channels (6, 7) and cytochrome P450 (7). These properties suggest that NNC or similar derivatives may hold promise for clinical development.

The current study assessed the effect of mibefradil and NNC on MB cells and evaluated their mechanism of action. For the first time, this study shows that CaV3 inhibitors, mibefradil and NNC, induce apoptosis that is associated with altered metabolic activity in MB cells. This work provides new insights into the mechanism of action of mibefradil and NNC, and may pave the way to test these molecules and/or their analogues in *in vivo* pre-clinical models to assess their suitability as a potential treatment options for MB.

Materials And Methods

Cell culture

MB cell lines, D341 Med (HTB-187™), CHLA-01-MED (CRL-3021™), and CHLA-01R-MED (CRL-3034™) were purchased from the American Type Culture Collection (ATCC) and cultured according to the supplier's recommendation. D341 cells were cultured in Minimum Essential Medium Eagle (EMEM- M0643, Life Technologies, CA, USA) supplemented with 20% foetal bovine serum (FBS). CHLA-01-MED and CHLA-01R-MED were cultured in Dulbecco's Modified Eagle's Medium/Nutrient Mixture F-12 Ham (D8900, Sigma-Aldrich, MO, USA) supplemented with B-27™ Supplement (Sigma-Aldrich, Ryde, NSW, Australia), 20 ng/ml basic FGF (Sigma-Aldrich), and 20 ng/ml EGF (Sigma-Aldrich). Cells were maintained at 37 °C in a humidified atmosphere of 5% CO2.

WST-1 assay

Metabolic activity of cells as a marker of cell viability and proliferation was assessed by WST-1 Cell Proliferation Assay Kit (10008883, Cayman Chemical, MICH, USA) according to the manufacture's recommendation. Three MB cell lines, D341, CHLA-01, and CHLA-01R, were used in this assay. Briefly, cells were seeded at a density of 30,000 cells/well in 96 well plates. 24 h later, treatment was added as shown in the results section. Assay reaction was assessed 24 or 72 h after treatment. For that, 10 µL of WST-1 reagent was added to each well for 4 h, absorption was measured using a plate reader (Multiskan Go, Thermo Fisher Scientific, Scoresby, VIC, Australia). Drugs used, including mibefradil dihydrochloride hydrate (M5441), NNC55-0396 hydrate (N0287), verapamil hydrochloride (V4629), nifedipine (N7634), vincristine (V0400000), and lomustine (L5918), *were purchased from* Sigma-Aldrich.

ATP level and protein content

For the assessment of cellular ATP levels, a luminescent ATP assay was employed. 3×10^4 cells were seeded in 100 µL per well in transparent 96-well plates and media and left to settle overnight.

Subsequently, drug treatments were added to cells for 72 h. Cells were then transferred to Eppendorf tubes and centrifuged for 3 min at 0.2 g. Following media removal, cells were washed with sterile phosphate-buffered saline (PBS) followed by another centrifugation to obtain cell pellet. For cell permeabilization, 40 µL of 0.5% Triton X-100/PBS was added to each tube for 10 min at room temperature. 10 µL of cell lysate was mixed with 90 µL assay buffer (300 µM d-luciferin, 5 µg/mL luciferase, 625 µM EDTA, 75 µM DTT, 6.25 mM $MgCl_2$, 25 mM HEPES, 1 mg/mL BSA in PBS, pH 7.4) in white 96-well plates, followed by immediate measurement of luminescence using a plate reader (Fluoroskan Ascent, Thermo Fisher Scientific). Protein content from cell lysates (10 µL) was quantified using the DC Protein Assay (500-0116; Bio-Rad, CA, USA) as recommended by the manufacturer. Absorbance at 750 nm was measured using *Multiskan Go Microplate Spectrophotometer (Thermo Fisher Scientific) and used for normalisation of ATP content in different treatments.*

Immunoblotting

For immunoblotting, 5 µg of total protein samples were resolved on a 10% Bis-Glycine-polyacrylamide gel and transferred onto Amersham™ Protran™ 0.2 µm Nitrocellulose (NC) blotting membrane (10600001, GE Healthcare). NC membranes were blocked in Tris-buffered saline with 0.1% Tween-20 (TBST) solution containing 5% (w/v) non-fat dry milk (NFDM) powder. Proteins were detected using primary antibodies rabbit polyclonal PARP (9542S, Sigma-Aldrich) at a 1:1000 dilution, rabbit monoclonal caspase-3 (ab32042, Abcam, Cambridge, UK) at a 1:1000 dilution, and mouse monoclonal glyceraldehyde 3-phosphate dehydrogenase (GAPDH) (G8795, Sigma-Aldrich) at a dilution of 1:10,000 as loading control. Secondary antibodies included horseradish peroxidase (HRP)–conjugated goat anti-rabbit (170-6515, Bio-Rad, 1:3000 dilution) and goat anti-mouse IgG (170-6516, Bio-Rad, 1:3000 dilution). Antibodies were prepared in 5% (w/v) NFDM powder dissolved in TBST solution. Anti-PARP and caspase-3 primary antibodies were incubated with membrane at 4° C overnight, while GAPDH and secondary antibodies were incubated at room temperature for 1 h. PageRuler™ Plus Prestained Protein Ladder (26620, Thermo Fisher Scientific) was used to ease detection of the molecular sizes (in kDa) of protein bands. Amersham™ ECL™ Prime Western Blotting Detection Reagent (RPN2236, GE Healthcare) was used to detect proteins. Digital images were recorded using the Amersham™ Imager 600 (29083461, GE Healthcare). Density of bands were quantified using Image Lab™ Software (version 6.0.1, Bio-Rad) and normalized to GAPDH.

Sphere generation

Spheroid generation was carried out by seeding CHLA-01R cells at 1×10^4 cells per well in 200 µL volume in round bottom 96 Ultra-Low Attachment Microplate (Product number 7007, Corning, MA, USA). Spheroid formation was initiated by centrifugation of the plate at 1000 g for 10 min and the plate was incubated at 37 °C and 5% CO_2 for five days until spheres were formed.

Propidium iodide (PI) incorporation and dual live/dead viability assays

To assess cell membrane integrity, as a marker of cell death, PI fluorescent staining was performed using PI dye. PI is impermeable to the intact plasma membrane and therefore will only bind to DNA of cells with compromised cell membrane. To stain MB spheres, 100 µL of media were removed from each well and PI at a concentration of 40 µg/mL in PBS (100 µL) was added to the treated spheres and analysed under fluorescent microscope (IN Cell Analyzer 2000, GE Healthcare, IL, USA). ImageJ 1.49q software (NIH, Bethesda, MD, USA, website: https://imagej.nih.gov/ij/) was used to analyse PI incorporation by measuring the signal intensity of the sphere from the images. For live/dead dual staining, treated spheres were dissociated into single-cell suspension using Accutase solution (A6964, Sigma-Aldrich). Subsequently, cells were washed with PBS and stained with 3 µM calcein-AM (Thermo Fisher Scientific) and propidium iodide (5 µM) followed by incubation for 30 min. 100 µl of cell suspension was transferred to black plates and imaged with fluorescent microscope (IN Cell Analyzer 2000) using excitation of 475 nm /emission of 511 nm for calcein-AM and excitation of 542 nm /emission of 620 nm for PI. Generated images were automatically analysed using IN Carta Image Analysis Software (GE Healthcare).

Assessment of mitochondrial membrane potential

Detection of altered mitochondrial membrane potential was performed using 5,5',6,6'-tetrachloro-1,1',3,3'-tetraethylbenzim-idazolylcarbocyanine iodide (JC-1) Mitochondrial Membrane Potential Assay Kit (ab113850, Abcam) according to the manufacturer's instructions. Briefly, MB cells were washed twice and incubated with the assay solution containing JC-1 dye (10 µM) for 30 min. Cells were then washed, suspended in assay buffer (supplemented with 5% FBS) and seeded at 6×10^4 in 50 µL in a black 96-well plate. 50 µl of 2× concentration of treatments, including different concentrations of mibefradil, NNC, Carbonyl cyanide 4-trifluoromethoxy phenylhydrazone (FCCP) as a positive control, or no treatment control, were added to cells followed by incubation at 37 °C for 6 h. Cells were imaged using IN Cell Analyzer 2000 (excitation wavelength used was 475 nm and emission wavelengths was 511 nm and 587 nm for the monomer and the aggregates of JC-1 molecules respectively). Images were analysed using IN Carta Image Analysis Software (GE Healthcare).

Measurement of cytosolic free Ca^{2+}

Cytosolic free Ca^{2+} levels were measured using Ca^{2+} indicator Fluo-4 (Fluo-4 NW Calcium Assay Kit, F36206, Invitrogen) according to the manufacturer's protocol. Briefly, MB cells D341 and CHLA-01 were plated at 7.5×10^4 *in 100 µL per well in a black plate 96-well plate (µClear®, Greiner, Germany) coated with poly-L-lysine (P4832, Sigma-Aldrich, Australia). After overnight incubation, cells were washed twice with the assay buffer (*1.26 mM calcium chloride, 0.49 mM magnesium chloride, 0.40 mM magnesium sulfate, 5.33 mM potassium chloride, 0.44 mM potassium phosphate monobasic, 4.16 mM sodium bicarbonate, 137.9 mM sodium chloride, 0.33 mM sodium phosphate dibasic anhydrous) and loaded with the dye solution for 50 min at 37 °C and 10 min at room temperature. Dye solution was removed, and cells were washed with the assay buffer (same as above excluding calcium chloride). For treatment, NNC (3.5-20 µM) in 0.5 mM BAPTA (B1214, Thermo Fisher Scientific) was added for 10 min in Ca^{+2} free

buffer. Fluorescence (excitation at 475 nm and emission at 525 nm) was measured at 20°C using a plate reader (Tecan Infinite M Nano, Tecan Austria GmbH).

Proteomic analysis

MB cell line, CHLA-01, was seeded at 3×10^5 cells per well in 12-well plate. After overnight incubation, cells were treated with different concentration of mibefradil (0, 3.5, and 7.5 µM) for 72 h. Cells were washed with PBS and lysed using chilled lysis buffer, 100 mM NaCl, 1% IGEPAL®, 0.5% sodium deoxycholate, 50 mM Tris (pH 8.0), 1× protease inhibitor (Roche Diagnostic GmbH, Germany), 1× phosphatase inhibitor (Roche Diagnostic GmbH, Germany). Protein concentrations were determined using Bio-Rad DC Protein Assay as described above.

Aliquots of 30 mg protein were sequentially reduced using 10 mM DTT overnight at 4 °C, alkylated using 50 mM iodoacetamide for 2 h at ambient temperature and then digested with 1.2 mg proteomics-grade trypsin/LysC (Promega) according to the SP3 protocol (8). Digests were halted by the addition of TFA to 0.1% and peptides collected by centrifugation at 21,000× g for 20 minutes. Samples were desalted using ZipTips (Merck) according to manufacturer's instructions. Proteomic analysis deployed a combination of data-dependent acquisition (DDA) and data independent acquisition (DIA) methods on a Q-Exactive HF and Ultimate 3000 RSLCnano LC/MS system (Thermo Scientific, Massachusetts, USA).

First, a project-specific spectral library was generated using off-line high-pH reversed phase HPLC peptide fractionation. A pooled digest (~180 mg peptide) was desalted using Pierce desalting spin columns (Thermo Scientific), evaporated to dryness and finally resuspended in 25 ml HPLC loading buffer (2 % acetonitrile containing 0.05 % TFA). Peptides were separated on a 100 × 1 mm Hypersil GOLD (particle size 1.9 mm) HPLC column (Thermo Scientific) using an Ultimate 3000 RSLCnano system with microfractionation and automated sample concatenation enabled. The HPLC was operated at 30 mL/min using a 40 min linear gradient of 96% mobile phase A (water containing 1% triethylamine, adjusted to pH 9.6 using acetic acid) to 50% mobile phase B (80% acetonitrile containing 1% triethylamine), followed by 6 min washing in 90% B and re-equilibration in 96% A for 8 min. Sixteen concatenated fractions were collected into 0.5 mL Protein lo-bind Eppendorf tubes, evaporated to dryness then reconstituted in 12 mL HPLC loading buffer.

Peptide fractions were analysed using 90 min nanoflow HPLC gradient and a Top15 DDA-MS method as previously described (9). Individual peptide samples (~1 mg peptide) were analysed by DIA-MS using 26 × 25 amu sequential MS2 scans over the range of 397.5-1027.5 m/z, with 1 amu overlap between windows between MS1 spectra (390 - 1240 m/z) acquired at 120k resolution. MS2 spectra were acquired at a resolution of 30,000 using an AGC target of 1e6, maximum IT of 55 ms and normalized collision energy of 27.

DDA- and DIA-MS raw files were processed using Spectronaut software (version 13.12, Biognosys AB, Switzerland). The project-specific library was generated using the Pulsar search engine to search DDA MS2 spectra against the UniProt Homo sapiens protein sequence database using Biognosys (BGS)

software factory settings, including N-terminal acetylation and methionine oxidation as variable modifications and cysteine carbamidomethylation as a fixed modification, up to two missed cleavages allowed and peptide, protein and PSM thresholds set to 0.01. Retention time alignment was based on the high precision iRT concept (10).With the exception that single-hit proteins were excluded, BGS factory settings were also used for relative quantitation between samples using the MaxLFQ algorithm (in Spectronaut version 15) for protein label-free quantitation and global normalization based on median MS2 intensity values.

Statistics and bioinformatics analysis

Proteins identified as candidates in Spectronaut (Supplemental Table S1) were imported into Perseus software (http://coxdocs.org/doku.php?id=perseus:start) for further processing. Label-free quantitation (LFQ) values were first log2 transformed and proteins with missing values were removed before using an unpaired *t*-test for statistical analysis. Proteins with altered expression of ±1.5 fold-change and false discovery rate (FDR)-adjusted *p* values below 0.05 compared to the control (Supplemental Table S2) were considered significant and selected for the enrichment analysis. Statistical overrepresentation test of significantly altered proteins was conducted using PANTHER online tool (11) with GO Biological Process annotation. Statistical analysis was performed using GraphPad Prism (version 8.0, GraphPad Software, Inc., San Diego, CA). Details of statistical analyses are provided in the corresponding figure legends.

Results

To assess the effect of mibefradil on MB cells, we treated three MB cell lines (D341, CHLA-01 and CHLA-01R) with increasing concentrations of mibefradil and assessed toxicity using WST-1 and ATP assays. Mibefradil treatment led to increased toxicity in all three cell lines in a concentration dependent manner in both WST-1 (Fig. 1A) and ATP (Fig. 1B) assays as endpoints. This toxicity was more pronounced in CHLA-01 cells.

Combination therapy is one approach to enhance the effect of current treatment options (eg. chemo/radio therapies) and/or for dose reductions to reduce side effects. We therefore explored the effect of mibefradil co-treatment with the clinically used MB chemotherapeutic agents, vincristine and lomustine in D341 and CHLA-01 cells. Low mibefradil concentrations by themselves did not significantly affect MB growth. However, combined with vincristine, mibefradil improved the ability of vincristine to suppress MB cell growth. Indeed, combining vincristine with 3.5 µM mibefradil, reduced the IC_{50} of vincristine around 3.5-times in D341 (from 5.03 nM to 1.47 nM, Fig. 2A) and 8-times in CHLA-01 cells (from 0.16 nM to 0.02 nM, Fig. 2B). Intriguingly, this synergistic effect was not seen with lomustine (Fig. 2C-D).

Since at this point it was unclear if the observed toxicity represented metabolic toxicity or cell death, we assessed whether mibefradil induces cell death in MB cells. Treatment of CHLA-01R cell spheres with increasing concentrations of mibefradil induced cell death as indicated by propidium iodide (PI) staining

(Fig. 3A). In a follow-up experiment, to ensure homogeneous distribution of the fluorescent dye to cells, subsequent to drug treatments, spheres were dissociated into single cell suspensions. Mibefradil induced a concentration-dependent decrease in calcein-AM and a simultaneous increase in PI staining, indicative of induction of cell death (Fig. 3B).

To assess whether the observed effect of mibefradil on MB cell growth was specific to T-type channel blockers, CHLA-01 cells were treated with mibefradil, its analogue, NNC55-0396 (NNC), or with L-type channel blockers, nifedipine and verapamil. L-type inhibitors did not affect MB cell growth to the same extent as T-type inhibitors (Fig. 4). Indeed, the L-type channel blockers only showed significant effects at the highest concentration tested (30 μM). Interestingly, NNC showed a greater inhibitory effect compared to mibefradil, with concentrations as low as 1.5 μM showing a significant effect (Fig. 4). Treatment of MB cells with NNC, also concentration-dependently reduced constitutive Ca^{2+} influx, as well as store operated Ca^{2+} entry (Fig. S1), indicating that CaV3 proteins are active Ca^{2+} channels in MB cells.

Although CaV3 inhibition resulted in cell death, the mechanism was unclear from this data, which cell death mechanism (12) was present. Apoptosis is a key mechanism of cell death that has been utilised as a target of many treatment strategies (13). To explore whether the observed cell death was via apoptosis, the expression of two apoptotic markers, Caspase-3 and cleaved poly(ADP-ribose) polymerase (PARP) was assessed after treatment of MB cells with NNC alone or in combination with vincristine. NNC alone significantly increased PARP degradation only at the highest concentration tested (7.5 μM), an effect that did not reach statistical significance for activated caspase-3 expression (Fig. 5). Vincristine alone (10 nM), enhanced PARP cleavage but did not significantly activate caspase-3. In contrast, the combination of NNC and vincristine significantly and synergistically enhanced both PARP cleavage and caspase-3 activation to a much higher extent compared to vincristine or NNC alone (Fig. 5). This suggested that NNC and its combination with vincristine induces apoptotic cell death.

Understanding the apoptotic mechanism is critical and can contribute to the development of drugs that target selective apoptotic pathways. Therefore, we used proteomics to further investigate the mechanistic effects of CaV3 inhibition in MB cells. In total, 4,819 protein groups were quantified across all samples. Principal component analysis of the LFQ data indicated clear separation of control and treated sample groups, although the individual samples did not cluster tightly (Fig. 6A). According to stringent criteria (FDR-adjusted p value <0.05 and fold-change >1.5) 120 and 106 proteins were significantly decreased or increased by mibefradil, respectively (displayed as a heat map in Fig. 6B and listed in Table S2). Pathway enrichment analysis of the proteins significantly decreased by mibefradil treatment (Table S3), showed they mainly belong to mitochondrial oxidative phosphorylation (OXPHOS) and ATP generation processes (Fig. 6C). In contrast, proteins significantly increased with mibefradil were mainly associated with sterol and lipid metabolism processes (Fig. 6C). These data suggest an altered energy metabolism in MB cells as a result of mibefradil treatment.

Given the suggested affected OXPHOS and ATP generation pathways by mibefradil, we next assessed intracellular ATP levels after treatment of cells with CaV3 inhibitors, mibefradil and NNC. To distinguish

between ATP generated from glycolysis or OXPHOS, in addition to normal growth of cells in the presence of glucose, galactose-containing media was used (14). Treatment of CHLA-01 cells with mibefradil or NNC reduced intracellular ATP levels in a concentration dependant manner in both glucose and galactose media (Fig. 7A-B). This reduction was more pronounced in galactose media, suggesting potential effects on mitochondrial OXPHOS. This result supported the proteomics data and prompted further experiments to assess the effect of CaV3 inhibitors on the mitochondrial function. To further investigate the effect of mibefradil and NNC on mitochondrial function, mitochondrial membrane potential was assessed. Accumulation of the polymeric form of JC-1 (red fluorescent aggregates) indicates high uptake of the stain into mitochondria, corresponding to high mitochondrial membrane potential (15). Treatment with 10 µM mibefradil resulted in a modest but statistically significant reduction in the membrane potential of CHLA-01 and D341 cells (Fig. 7C-D). NNC treatment, significantly reduced mitochondrial membrane potential in both CHLA-01 and D341 cells at 7.5 and 10 µM in a concentration-dependent manner (Fig. 7C-D). Trifluoromethoxy carbonylcyanide phenylhydrazone (FCCP), an uncoupler of the mitochondrial OXPHOS, was used as positive control. FCCP suppressed mitochondrial membrane potential in D341 cells, but not to the same extent compared to NNC (Fig. 7D). These data suggest that CaV3 inhibitors directly affect mitochondrial function as a potential mechanism to induce cell toxicity by an apoptotic mechanism.

Discussion

This study identified and explored the selective toxicity of the CaV3 inhibitors, mibefradil and NNC, on MB cells. Our data demonstrated that both compounds lead to apoptotic cell death in MB cells, alone or in combination with the clinically used chemotherapeutic vincristine. This CaV3 inhibitor-induced cytotoxicity was associated with a reduced intracellular ATP levels and mitochondrial function, indicated by a disruption of mitochondrial membrane potential. It is, however, still unclear how these compounds affect mitochondrial function in detail. Mitochondria plays a critical role in the regulation of intracellular Ca^{2+} homeostasis. Mitochondria take up intracellular Ca^{2+} from the endoplasmic reticulum or from an influx of extracellular Ca^{2+} to prevent cytoplasmic Ca^{2+} overload. Conversely, this mitochondrial Ca^{2+} directly regulates mitochondrial function and affects ATP synthesis (16, 17). Given the disruption of mitochondrial membrane potential by CaV3 inhibitors, it will be of interest to explore mitochondrial Ca^{2+} levels after exposure of cells to mibefradil and NNC in future studies. This can be achieved using mitochondria-specific genetically-encoded Ca^{2+} indicators (17) or small molecule fluorescent dyes that localise to mitochondria, such as Rhod-2 (18).

This study also identified that CaV3 inhibitors sensitised MB cells to the clinically used chemotherapeutic, vincristine. MB is a difficult cancer to treat, and chemotherapy treatment for MB is associated with considerable toxicities and potential long-term disabilities. Indeed, vincristine displays significant neurotoxic side effects in children including peripheral neuropathies and seizures (19, 20). One possible approach to ameliorate side effects of vincristine is to decrease the total dose used. Our observed synergistic effects of CaV3 inhibitors and vincristine are the first step to explore whether this novel

combinatory strategy may provide increased treatment efficacy, while at the same time decreasing vincristine-associated adverse effects. Future studies are also warranted to understand the molecular mechanism of this synergistic effect. Vincristine is known to induce cell death via cell-cycle dependent mechanisms in particular in G1 and S phase (21). Calcium signalling, on the other hand, plays a critical role in the control of cell cycle through multiple checkpoints (22). Given this association, future studies should explore the effect of CaV3 inhibitors on cell cycle phases in combination with vincristine.

This study did not assess whether the effect of mibefradil and NNC is mediated by a specific CaV3 channel. Mibefradil, is a broad T-type calcium channel blocker and weak L-type calcium channel blocker (23), while NNC blocks CaV3.1 and CaV3.2 (6, 24). Further studies, using siRNA-mediated silencing are warranted to assess the effect of each of the CaV3 isoforms on MB growth and metabolic activities.

Mibefradil recently successfully completed a Phase I trial for recurrent high-grade glioma**.** In combination with temozolomide, mibefradil was well-tolerated and showed no toxicity (NCT01480050) (5). In another Phase I dose expansion trial, mibefradil was safely co-administered with hypofractionated radiation therapy over a 17-day period at 200 mg/day in patients with recurrent glioblastoma (NCT02202993)(25). As discussed, NNC, an analogue of mibefradil, possesses multiple advantages compared to mibefradil that makes it attractive for potential future clinical trials. Our studies here showed that NNC is more effective than mibefradil in inducing toxicity in MB cells. This could be due to the enhanced selectivity of NNC on inhibition of T-type channels compared to mibefradil (6). Future studies can work towards testing mibefradil and NNC in *in vivo* models of MB to assess their efficacy in suppression of tumour progression.

Overall, this study demonstrated that the CaV3 inhibitors, mibefradil and NNC alter metabolism and induce apoptotic cell death in MB cells. Future studies need to test mibefradil and NNC, as well as their analogues in *in vitro* and *in vivo* models to explore the possibility of using these compounds as potential future treatment strategies against MB.

Declarations

Ethics approval

Not applicable.

Consent for publication

Not applicable.

Availability of data and material

The DIA-MS and DDA-MS raw data and Spectronaut pivot reports including the complete sets of identified peptides and proteins are available at ProteomExchange (dataset PDX026988) with reviewer

login and password: reviewer_pxd026988@ebi.ac.uk; Pfc4cgjc.

Competing interests

Authors declare no conflict of interest.

Funding

This research was funded by the Brain Foundation, Kids Cancer Project and Research Enhancement Program of the College of Health and Medicine, University of Tasmania.

Author contributions

Conceptualization: Iman Azimi, Mohammed Sedeeq, Nuri Gueven; Methodology: Mohammed Sedeeq, Ahmed Maklad, Zikai Feng, Richard Wilson; Formal analysis and investigation: Mohammed Sedeeq, Ahmed Maklad, Richard Wilson, Iman Azimi; Writing - original draft preparation: Iman Azimi, Mohammed Sedeeq, Nuri Gueven; Writing - review and editing: Mohammed Sedeeq, Ahmed Maklad, Zikai Feng, Richard Wilson, Nuri Gueven, Iman Azimi; Funding acquisition: Iman Azimi; Supervision: Iman Azimi, Nuri Gueven.

Acknowledgements

Not applicable.

Compliance with Ethical Standards

Not applicable.

Consent to Participate

Not applicable.

References

1. Ramaswamy V, Remke M, Bouffet E, Bailey S, Clifford SC, Doz F, et al. Risk stratification of childhood medulloblastoma in the molecular era: the current consensus. Acta neuropathologica. 2016;131(6):821-31.

2. Maddrey AM, Bergeron JA, Lombardo ER, McDonald NK, Mulne AF, Barenberg PD, et al. Neuropsychological performance and quality of life of 10 year survivors of childhood medulloblastoma. Journal of Neuro-oncology. 2005;72(3):245-53.

3. Sedeeq M, Maklad A, Gueven N, Azimi I. Development of a high-throughput agar colony formation assay to identify drug candidates against medulloblastoma. Pharmaceuticals. 2020;13(11):368.

4. Zhang Y, Cruickshanks N, Yuan F, Wang B, Pahuski M, Wulfkuhle J, et al. Targetable T-type calcium channels drive glioblastoma. Cancer research. 2017;77(13):3479-90.

5. Holdhoff M, Ye X, Supko JG, Nabors LB, Desai AS, Walbert T, et al. Timed sequential therapy of the selective T-type calcium channel blocker mibefradil and temozolomide in patients with recurrent high-grade gliomas. Neuro-oncology. 2017;19(6):845-52.

6. Huang L, Keyser BM, Tagmose TM, Hansen JB, Taylor JT, Zhuang H, et al. NNC 55-0396 [(1S, 2S)-2-(2-(N-[(3-benzimidazol-2-yl) propyl]-N-methylamino) ethyl)-6-fluoro-1, 2, 3, 4-tetrahydro-1-isopropyl-2-naphtyl cyclopropanecarboxylate dihydrochloride]: a new selective inhibitor of T-type calcium channels. Journal of Pharmacology and Experimental Therapeutics. 2004;309(1):193-9.

7. Quesada A, Bui PH, Homanics GE, Hankinson O, Handforth A. Comparison of mibefradil and derivative NNC 55-0396 effects on behavior, cytochrome P450 activity, and tremor in mouse models of essential tremor. European journal of pharmacology. 2011;659(1):30-6.

8. Hughes CS, Moggridge S, Müller T, Sorensen PH, Morin GB, Krijgsveld J. Single-pot, solid-phase-enhanced sample preparation for proteomics experiments. Nature protocols. 2019;14(1):68-85.

9. Yen S, Song Y, Preissner M, Bennett E, Wilson R, Pavez M, et al. The proteomic response is linked to regional lung volumes in ventilator-induced lung injury. Journal of Applied Physiology. 2020;129(4):837-45.

10. Bruderer R, Bernhardt OM, Gandhi T, Miladinović SM, Cheng L-Y, Messner S, et al. Extending the Limits of Quantitative Proteome Profiling with Data-Independent Acquisition and Application to Acetaminophen-Treated Three-Dimensional Liver Microtissues*[S]. Molecular & Cellular Proteomics. 2015;14(5):1400-10.

11. Mi H, Ebert D, Muruganujan A, Mills C, Albou L-P, Mushayamaha T, et al. PANTHER version 16: a revised family classification, tree-based classification tool, enhancer regions and extensive API. Nucleic Acids Research. 2021;49(D1):D394-D403.

12. Galluzzi L, Vitale I, Aaronson SA, Abrams JM, Adam D, Agostinis P, et al. Molecular mechanisms of cell death: recommendations of the Nomenclature Committee on Cell Death 2018. Cell Death & Differentiation. 2018;25(3):486-541.

13. Wong RS. Apoptosis in cancer: from pathogenesis to treatment. Journal of Experimental & Clinical Cancer Research. 2011;30(1):1-14.

14. Rossignol R, Gilkerson R, Aggeler R, Yamagata K, Remington SJ, Capaldi RA. Energy substrate modulates mitochondrial structure and oxidative capacity in cancer cells. Cancer research. 2004;64(3):985-93.

15. Reers M, Smiley ST, Mottola-Hartshorn C, Chen A, Lin M, Chen LB. [29] Mitochondrial membrane potential monitored by JC-1 dye. Methods in enzymology. 1995;260:406-17.

16. McCORMACK JG, Halestrap AP, Denton RM. Role of calcium ions in regulation of mammalian intramitochondrial metabolism. Physiological reviews. 1990;70(2):391-425.

17. Suzuki J, Kanemaru K, Iino M. Genetically encoded fluorescent indicators for organellar calcium imaging. Biophysical Journal. 2016;111(6):1119-31.

18. Fonteriz RI, de la Fuente S, Moreno A, Lobatón CD, Montero M, Alvarez J. Monitoring mitochondrial [Ca2+] dynamics with rhod-2, ratiometric pericam and aequorin. Cell calcium. 2010;48(1):61-9.

19. Macdonald DR. Neurologic complications of chemotherapy. Neurologic clinics. 1991;9(4):955-67.

20. von Bueren A, Von Hoff K, Benesch M, Rutkowski S. Dose reductions of vincristine in children with medulloblastoma treated in the maintenance arm of the prospective multicenter trial HIT'91. Klinische Padiatrie. 2009;221(6):396-7.

21. Kothari A, Hittelman WN, Chambers TC. Cell cycle–dependent mechanisms underlie vincristine-induced death of primary acute lymphoblastic leukemia cells. Cancer research. 2016;76(12):3553-61.

22. Humeau J, Bravo-San Pedro JM, Vitale I, Nuñez L, Villalobos C, Kroemer G, et al. Calcium signaling and cell cycle: progression or death. Cell calcium. 2018;70:3-15.

23. Martin RL, Lee J-H, Cribbs LL, Perez-Reyes E, Hanck DA. Mibefradil block of cloned T-type calcium channels. Journal of Pharmacology and Experimental Therapeutics. 2000;295(1):302-8.

24. Kim J-W, Oh HA, Lee SH, Kim KC, Eun PH, Ko MJ, et al. T-type calcium channels are required to maintain viability of neural progenitor cells. Biomolecules & therapeutics. 2018;26(5):439.

25. Lester-Coll NH, Supko JG, Kluytenaar J, Pavlik KF, Yu JB, Moliterno J, et al. Mibefradil dihydrochoride with hypofractionated radiation for recurrent glioblastoma: A phase I dose expansion trial. American Society of Clinical Oncology; 2018.

Figures

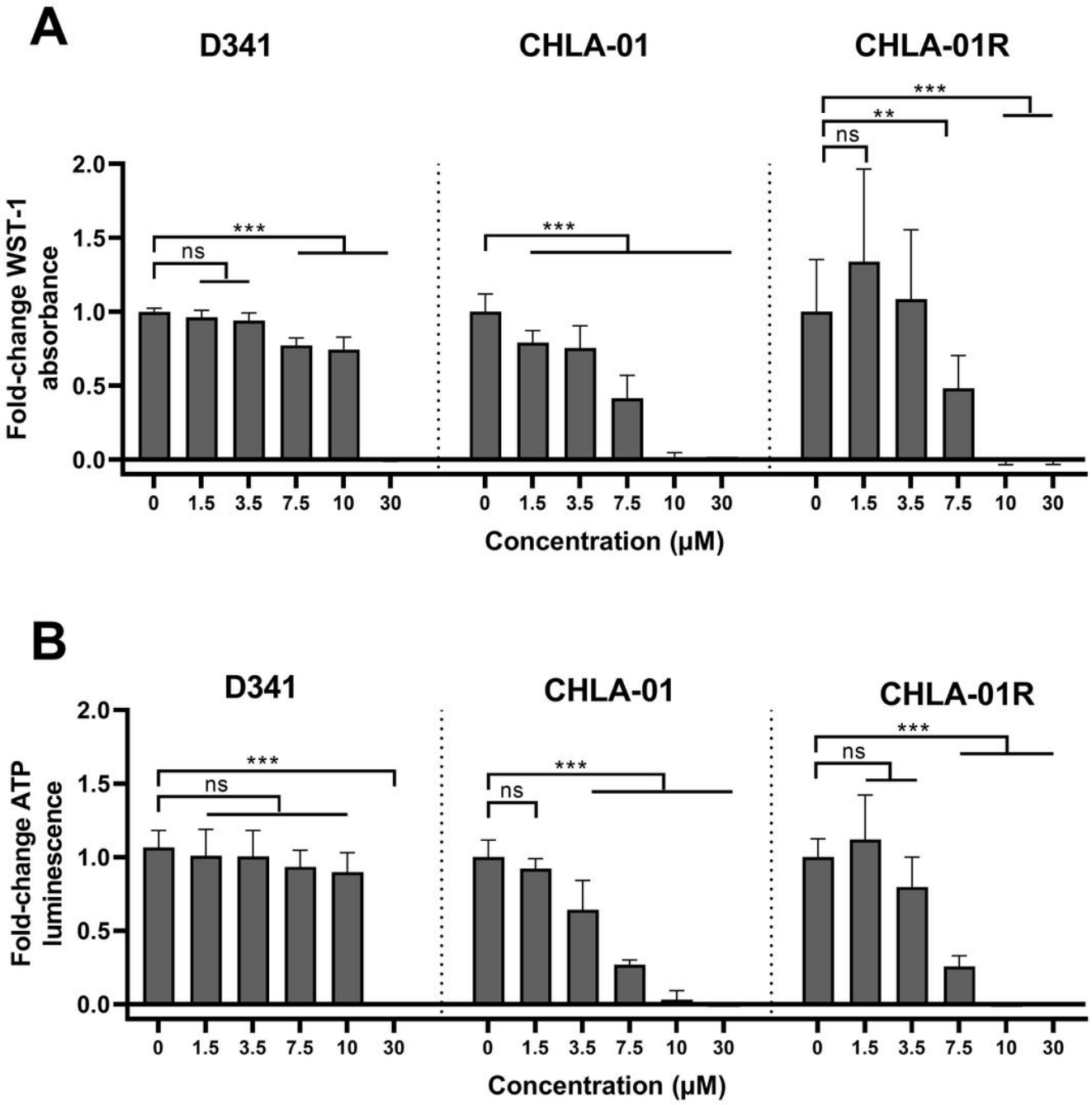

Figure 1

Mibefradil induces toxicity in MB cells. D341, CHLA-01 and CHLA-1R cells were treated with mibefradil for 72 h and subsequently assessed for toxicity by (A) WST-1 and (B) ATP assays. Data of each concentration was standardized to the non-treated control (0.1% DMSO) as fold change. Data expressed as mean ± standard deviation from three independent experiments with three replicates each. ns = not significant ($p>0.05$), ** $p<0.01$, *** $p<0.001$ (one-way ANOVA with Dunnett multiple comparisons test compared with the non-treated 0 control group).

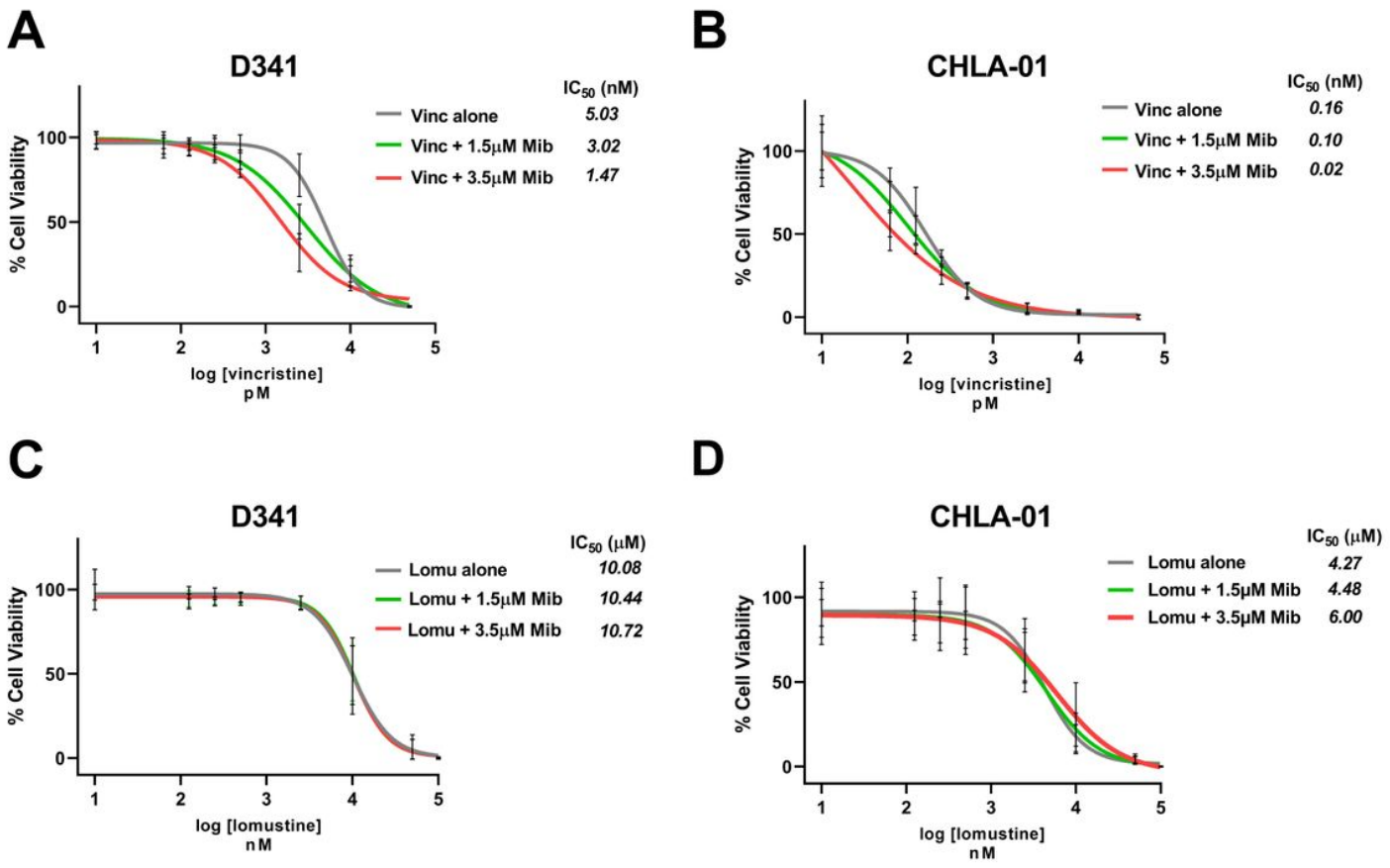

Figure 2

Cytotoxic effects of Mibefradil in combination with chemotherapeutics. D341 and CHLA-01 cells were treated with vincristine (0-50 nM) (A and B) or lomustine (0-100 μM) (C and D) alone or in combination with 1.5 and 3.5 μM mibefradil for 72 h before toxicity was assessed by WST-1 assay. Results for each concentration were standardized to the non-treated control and expressed as percent control. Data represents mean ± standard deviation from three independent assays with three replicates each. Mib: mibefradil. Vinc: vincristine. Lomu: lomustine.

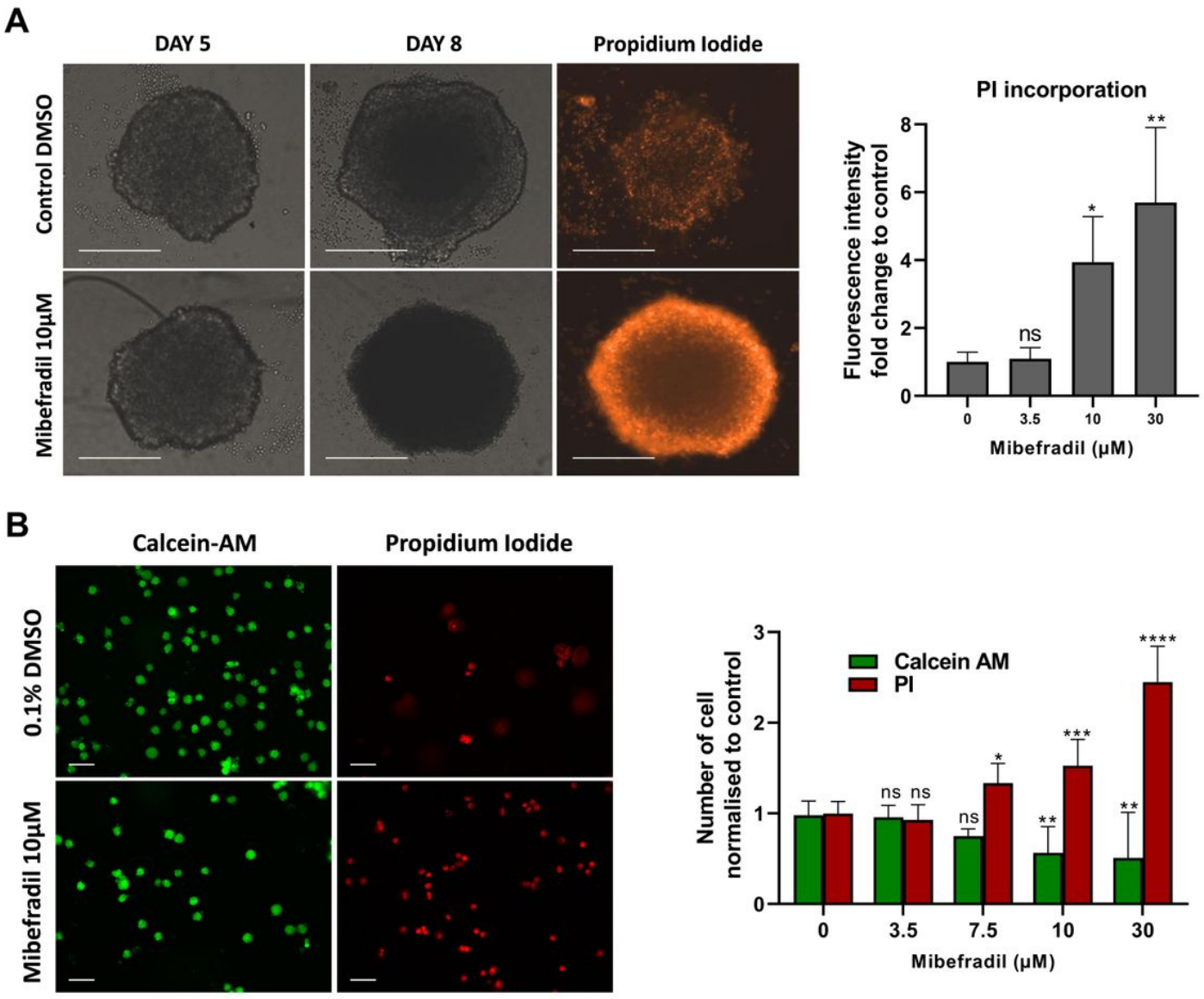

Figure 3

Mibefradil induces cell death in MB spheres. (A) Left panel: Representative bright field and fluorescent images of CHLA-01R cell spheres at before (day 5) and after (day 8) treatment with mibefradil (10 µM) or DMSO control. The scale bar is 300 µm. Right panel: quantitative analysis of PI fluorescence intensity of DMSO control and increasing concentrations of mibefradil. Results for each concentration were standardized to the non-treated control and expressed as fold change. Data represents mean ± standard deviation from three independent experiments with three replicates each. ns = not significant ($p>0.05$), * $p<0.01$, ** $p<0.001$, (one-way ANOVA with Dunnett multiple comparisons test compared with the non-treated 0 control group). (B) Live/dead analysis of MB spheres treated with different concentrations of mibefradil. Generated spheres were grown for 5 days and treated for 3 days. Single-cell suspension from dissociated spheres were stained with calcein-AM/propidium iodide and imaged using IN-Cell 2200 analyser (20x magnification). Left panel: Exemplary fluorescence images. Right panel: quantitative analysis of acquired images using IN Carta image analysis software. The scale bar is 60 µm. Results for

each concentration were standardized to the non-treated control and expressed fold change. Data expressed as mean ± standard deviation from three independent assays with three replicates each. ns = not significant (p>0.05), * p<0.05, ** p<0.01, *** p<0.001, **** p<0.0001 (two-way ANOVA with Dunnett multiple comparisons test compared with the non-treated control group).

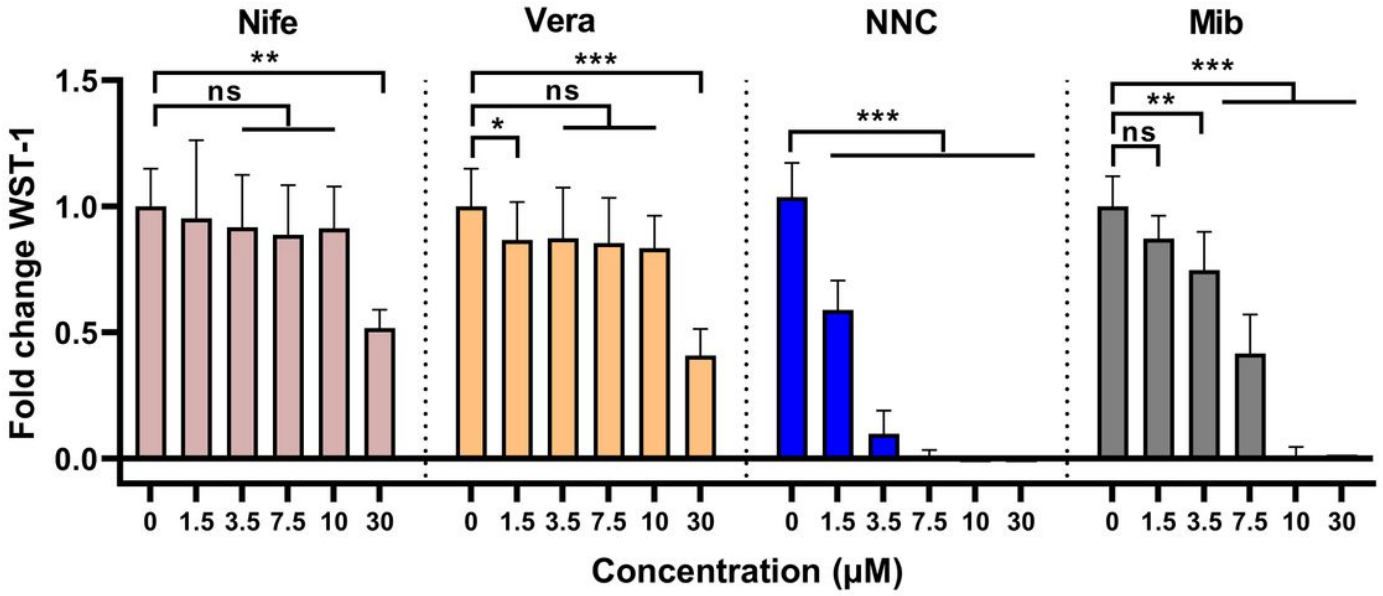

Figure 4

Blockade of T-type, but not L-type Ca2+ channels, reduces cell viability in MB cells. Viability of CHLA-01 cells, measured by WST-1 assay, treated for 72 h with increasing concentrations of Ca2+ channel antagonists. Results for each concentration were standardized to the non-treated control and expressed as fold change. Data expressed as mean ± standard deviation from three independent assays with three replicates each. ns = not significant (p>0.05), * p<0.05, ** p<0.001, *** p<0.0001 (two-way ANOVA with Dunnett multiple comparisons test compared with the non-treated 0 control group). Nife: nifedipine. Vera: verapamil. Mib: mibefradil.

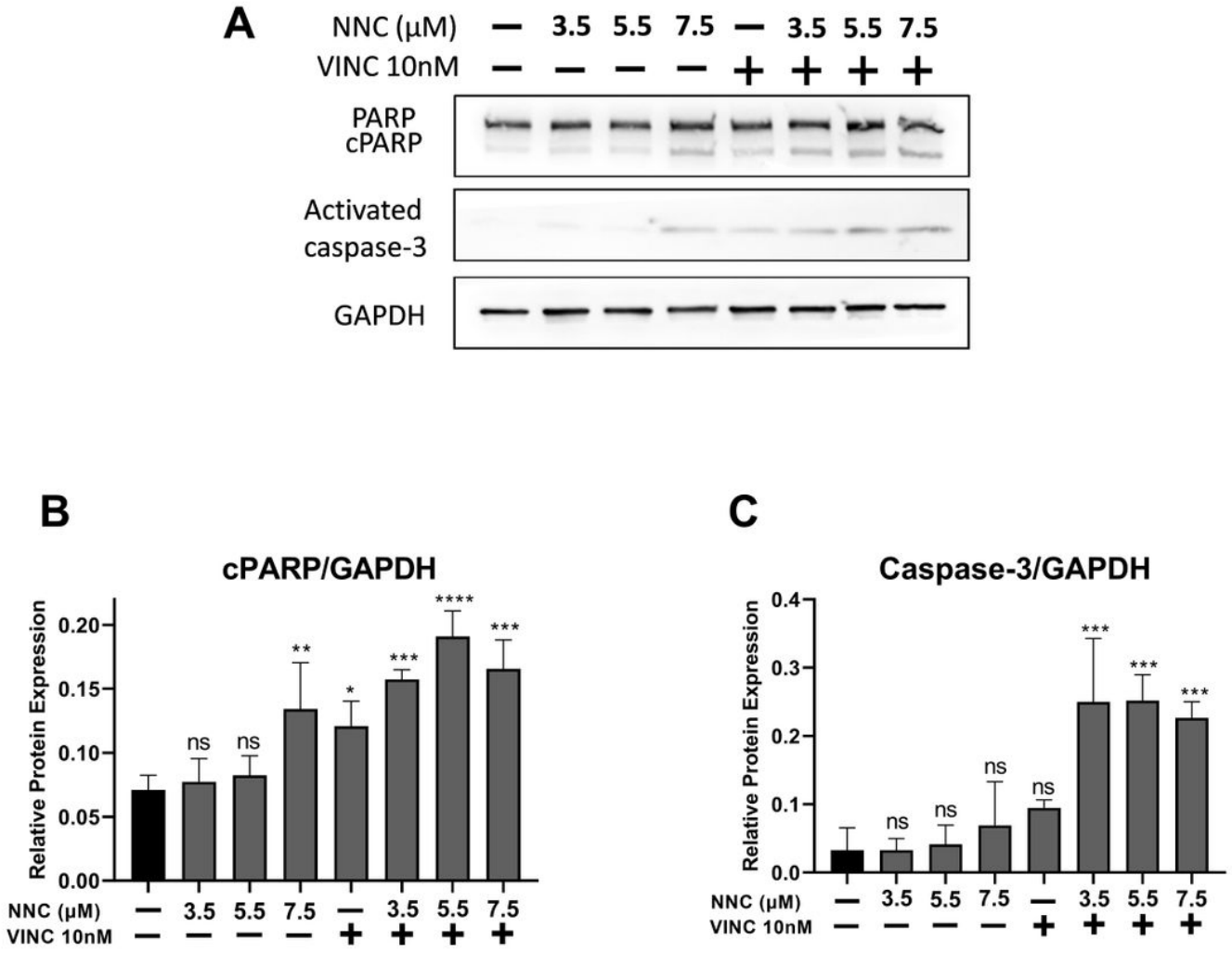

Figure 5

Effect of NCC on apoptotic cell death. D341 cells were treated for 12 h with different concentrations of NNC (0 - 7.5 μM), or vincristine (Vinc, 10 nM) alone or in combination. (A) Representative immunoblot of the cleaved PARP (cPARP), caspase-3 and GAPDH. Densitometric analysis of total (B) Cleaved PARP (cPARP) and (C) activated caspase-3 (both normalized to GAPDH as loading control). (ns: not significant $p > 0.05$, * $p < 0.05$, ** $p < 0.01$, *** $p < 0.001$, one-way ANOVA, with Dunnett multiple comparisons test compared with control (c) group), n = 3. Bars present mean ± standard deviation from three independent experiments.

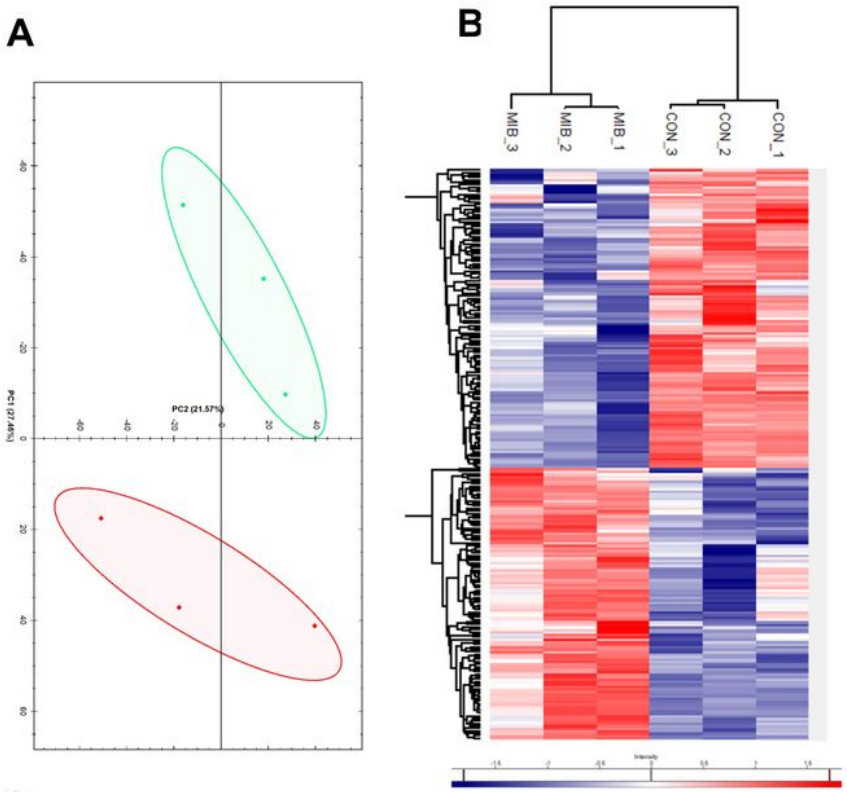

C

Decreased proteins				
GO biological process complete	**Count**	**Fold Enrichment**	**P value**	**FDR**
Aerobic respiration	23	24.67	1.80E-24	2.85E-20
Oxidative phosphorylation	21	30.03	5.29E-24	4.18E-20
Cellular respiration	23	21.11	4.59E-23	2.42E-19
Respiratory electron transport chain	20	30.65	4.74E-23	1.87E-19
Mitochondrial ATP synthesis coupled electron transport	19	35.06	6.37E-23	2.01E-19
ATP synthesis coupled electron transport	19	35.06	6.37E-23	1.68E-19
Electron transport chain	22	22.21	1.58E-22	3.58E-19
Cellular metabolic process	96	2.18	4.52E-22	8.94E-19
Aerobic electron transport chain	18	35.11	9.08E-22	1.59E-18
Energy derivation by oxidation of organic compounds	23	15.42	3.17E-20	5.02E-17

Increased proteins				
GO biological process complete	**Count**	**Fold Enrichment**	**P value**	**FDR**
Secondary alcohol biosynthetic process	16	75.58	3.87E-24	6.12E-20
Cholesterol biosynthetic process	16	75.58	3.87E-24	3.06E-20
Sterol biosynthetic process	16	65.72	2.48E-23	1.30E-19
Alcohol biosynthetic process	17	32.78	2.86E-20	1.13E-16
Cholesterol metabolic process	18	27.21	4.17E-20	1.32E-16
Steroid biosynthetic process	18	26.99	4.75E-20	1.25E-16
Secondary alcohol metabolic process	18	25.19	1.46E-19	3.29E-16
Sterol metabolic process	18	24.12	2.96E-19	5.85E-16
Small molecule biosynthetic process	26	9.27	9.12E-18	1.60E-14
Steroid metabolic process	20	14.26	3.67E-17	5.80E-14

Figure 6

Proteomic analysis with mibefradil treatment. (A) Principal component analysis of the proteomics data showing control samples in red and treated samples in green (B) hierarchical cluster analysis of significant proteins according to Z-scored LFQ values (C) Statistical overrepresentation test of proteins that were significantly increased (106 proteins, Table S2) or decreased (120 proteins, Table S2) by treatment of CHLA-01 MB cells with mibefradil (7.5 μM) for 72 h compared to the control. PANTHER

online tool (11), and GO Biological Process annotation were utilised. Fisher's Exact test and False Discovery Rate (FDR) calculation were used for data analysis. Top 10 biological processes are shown. Complete list of the biological processes is shown in Table S3.

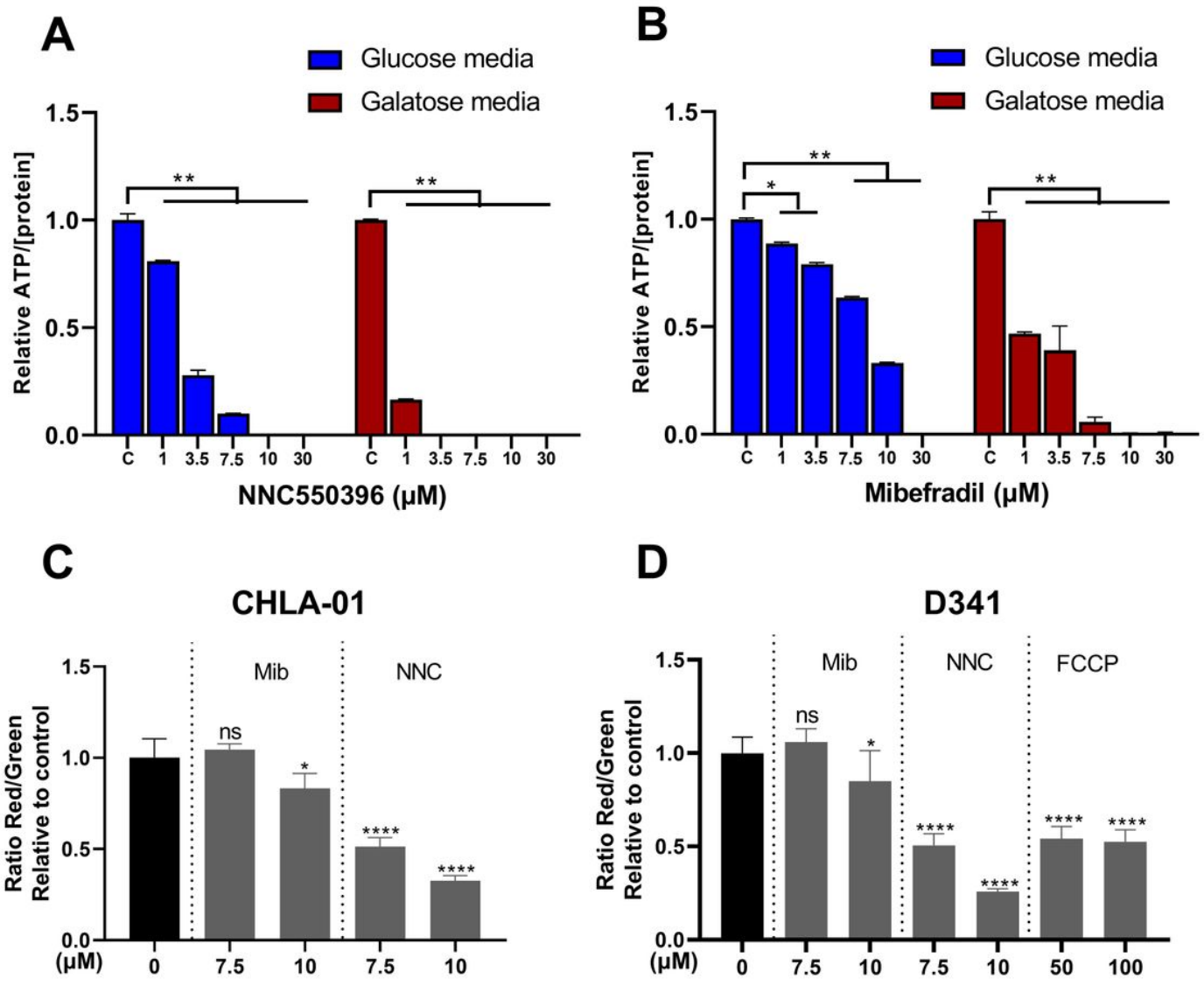

Figure 7

Effects of mibefradil and NNC on cellular ATP levels and mitochondrial membrane potential. (A-B) CHLA-01 cells were treated for 24 hr with increasing concentration of (A) NNC and (B) mibefradil (0-30 μM) in the presence of glucose (blue) or galactose (red) media before ATP levels were quantified from cell lysate. All data were normalised to protein content. Data were expressed as mean ± standard deviation from three independent assays with three replicates each, * $p<0.05$, ** $p<0.0001$ (two-way ANOVA with Dunnett multiple comparisons test compared with the non-treated 0 control group). (C-D) Mitochondrial membrane potential was quantified using JC-1 fluorescence. (C) CHLA-01 and (D) D341 MB cells were stained with JC-1 dye and treated with NNC, mibefradil or control for 6 h. Cells were analysed using IN Cell Analyzer 2200 using FITC and Cy3 filter sets. Data were expressed as mean ± standard deviation

from three independent assays with three replicates each. ns = not significant ($p>0.05$), * $p<0.05$, *** $p<0.001$, **** $p<0.0001$ (one-way ANOVA with Dunnett multiple comparisons test compared with the non-treated 0 control group).

Supplementary Files

This is a list of supplementary files associated with this preprint. Click to download.

- SupplementalTables.xlsx
- SupplementaryFigS1.pdf